International Journal of Pavement Engineering

ISSN: 1029-8436 (Print) 1477-268X (Online) Journal homepage: http://www.tandfonline.com/loi/gpav20

Measurement method of asphalt pavement mean texture depth based on multi-line laser and binocular vision

Xinzhuang Cui, Xinglin Zhou, Junjie Lou, Jiong Zhang & Maoping Ran

To cite this article: Xinzhuang Cui, Xinglin Zhou, Junjie Lou, Jiong Zhang & Maoping Ran (2015): Measurement method of asphalt pavement mean texture depth based on multi-line laser and binocular vision, International Journal of Pavement Engineering, DOI: 10.1080/10298436.2015.1095898

To link to this article: http://dx.doi.org/10.1080/10298436.2015.1095898

Published online: 05 Nov 2015.

INTERNATIONAL JOURNAL OF PAVEMENT ENGINEERING, 2015
http://dx.doi.org/10.1080/10298436.2015.1095898

Taylor & Francis
Taylor & Francis Group

Measurement method of asphalt pavement mean texture depth based on multi-line laser and binocular vision

Xinzhuang Cui[a], Xinglin Zhou[b], Junjie Lou[a], Jiong Zhang[a] and Maoping Ran[b]

[a]School of Civil Engineering, Shandong University, Jinan, China; [b]School of Automobile and Traffic Engineering, Wuhan University of Science & Technology, Wuhan, P.R. China

ABSTRACT

A new measuring method of mean texture depth of asphalt pavement is proposed based on the technology of multi-line laser and binocular vision. The developed method is incorporated with the profile method and the digital image technology. A three-dimensional mathematical model is established based on the triangulation measuring principle in order to implement the three-dimensional reconstruction of asphalt surface profile. Image processing technology helps locate the exact coordinates of each point on the model. In addition, the techniques of multi-line laser pairing and epipolar restriction are introduced for the image matching between multi-line laser and binocular vision. Through the model and the spatial equations obtained, the values of the mean profile depth of asphalt pavement can be figured out. According to the profile method, an integrated calculation procedure of texture depth is established. A set of sand patch field tests are implemented to verify the reliability of the developed method.

ARTICLE HISTORY
Received 28 October 2014
Accepted 6 July 2015

KEYWORDS
Asphalt pavement; mean texture depth (MTD); multi-line laser; binocular vision; three-dimensional reconstruction; digital image processing

1. Introduction

Mean texture depth (MTD) is an essential parameter that mainly reflects the asphalt pavement performances of skid-resistance and noise level (Adams and Richard Kim, 2014). Novel measuring methods of MTD have been widely studied (Zelelew *et al*. 2013). Compared with the traditional contact measuring methods such as the sand patch test and the outflow meter, the advanced methods utilising non-contact techniques such as photometric stereo and laser techniques have demonstrated their advantages (Meegoda *et al*. 2013).

The photometric stereo technique, which has been used to recover three-dimensional shapes of objects, can be used to recover pavement surface texture (Ergun *et al*. 2005, El Gendy and Shalaby 2007, 2008, El Gendy *et al*. 2011). The system consists of a light source, a camera, a monitor, a video printer, a scanner, a computer and an X–Y table. The light source is assumed to be a point source and illuminate the sample cores surface placed on the X–Y table, which is used to directionally move sample cores and position them accurately under the camera. The camera captures a surface profile and shows it on the monitor. Results could be printed by the video printer and stored by means of the scanner and the computer. This technique is mainly used in laboratory tests and is temporarily not suitable for practical field tests because it is vulnerable to variation of illumination intensity, angle of incidence, ambient light and the shadow produced by aggregates.

Laser technique is another major application of non-contact measuring methods on pavement texture measurement. The circular track meter (CTMeter) is a type of laser-based device which has been widely used in texture measurement (Henry 2000, Abe *et al*. 2001, Noyce *et al*. 2007). The CTMeter has a laser displacement sensor mounted on an arm that rotates on a circumference with a 142 mm radius and measures the texture with a sampling interval of approximately 0.9 mm (ASTM E2157 2001). The mean profile depth (MPD) obtained by CTMeter has high correlation with the MTD measured by the sand patch method (Henry 2000, Flintsch *et al*. 2005). Comparatively, CTMeter is relatively expensive and time-consuming. CTMeter is limited to measure on the static circular track on which the discrete fourier transformation measures the dynamic coefficient of friction. Due to the fixed and relatively large sampling interval, CTMeter can only measure texture with longer wavelengths. Previous studies (Hanson and Prowell 2004, Prowell and Hanson 2005) indicated that the coefficient of variation for the CTMeter was 3.2 and 5.9% for repeatability and reproducibility, respectively. In some cases, CTMeter could be more variable than the minimum reported precision for the sand patch method. The study also found that previously developed equations for the CTMeter to predict texture were inadequate for the wide range of mix types and aggregate types, especially for the open-graded mixture pavement. Moreover, since the CTMeter measures texture in a circular ring, it is difficult to evaluate grooved surfaces with the CTMeter data (Byrum *et al*. 2010). Another practical obstacle of the CTMeter

CONTACT Xinglin Zhou tjfdw@sdu.edu.cn

is that it cannot collect data along a linear wheel path at higher speeds, which leads to low test efficiency in the field test. It also increases the exposure of operators to vehicles and thus to the risk of injury while measuring texture (Pidwerbesky *et al.* 2006).

A standard method for determining the MPD of the pavement texture from a pavement profile achieved by laser devices is provided in the ASTM Standard (ASTM E1845 2009).Vehicle-mounted laser devices have been developed to measure texture along the linear wheel path at highway speeds without interfering with traffic. These devices improve testing efficiency to a great degree while maintaining well correlation with the sand patch method or the CTMeter (McGhee and Flintsch 2003). A high value of frames per second of the image system provide abundant image samples and one clear image can be simultaneously recognised through computer. Therefore, vehicle-mounted laser devices are regarded as a good method to measure texture for pavement management from a practical perspective. However, it was not financially viable to develop a dedicated high-speed vehicle-mounted laser device for measuring texture (Vercoe 2002). The price of the device is fairly high because of the vehicle cost and its additional functions, such as pavement unevenness inspection and pavement damage recognition. In addition, the severe vibration of the vehicle suspension system has significant effect on testing precision, especially at high speeds. Usually, an accelerometer is installed on vehicle-mounted laser devices to record the vertical acceleration, so that the displacement of laser senor caused by the vehicle suspension vibration could be compensated. The attached accelerometer not only complicates the measuring system, but incurs the increasingly integral errors of the acceleration at low vibrating frequencies. Some existing vehicle-mounted laser devices, e.g. the profiling vehicles with ICC system (manufactured by International Cybernetics Corporation), employed lower-frequency lasers which failed in acquiring texture at a smaller sampling interval (McGhee and Flintsch 2003, Flintsch *et al.* 2005). It was also found that the profile measurements from those devices were affected by the testing speed (Choubane *et al.* 2002). Moreover, this type of devices applied a root-mean-square-based proprietary algorithm to calculate the MPD, which is not fully consistent with ASTM E1845.

In this study, an innovative method of the MPD measurement based on multi-line laser and binocular vision was proposed. Incorporating the digital image processing technology, this study introduced the technique of multi-line laser pairing and the epipolar constraints as a solution to binocular stereo matching. MTD can be estimated through MPD based on the profile method, which includes an empirical algorithm of the estimation of MTD. This measurement method has the advantages of three-dimensional digitisation, automation and simple operation. More than one 2D profiles of the pavement surface can be obtained to form a texture region. The vehicle-mounted device makes the measurement automatic and rapid. Field tests with the sand patch test were carried out in order to verify the feasibility of the proposed method.

2. Measuring system

The measuring system (as shown in Figure 1) consists of two charge-coupled device (CCD) cameras (installed at both sides), four or more multi-line laser generators and a computer. On the basis of the existing measuring technique of binocular vision, the introduction of multi-line laser aims to solve the problem of stereo matching.

Light planes intersect with the surface of asphalt pavement on which the multi-line striations are casted by the multi-line laser generators. As a result, a three-dimensional image of multi-line striations modulated by the texture forms on the surface. The three-dimensional image is shot, respectively, by the cameras on both sides, thus two-dimensional distorted images pair is captured and transmitted to the computer through a 1000 Mbps Ethernet port of the CCD cameras.

The image coordinates of the points on the contour of optical sections can be extracted in digital image processing. Homonymous image points, which mean the corresponding points, respectively, locate on the left and right images, are positioned by stereo matching utilising the multi-line laser. Based on the mathematical model established with the homonymous image points, a transfer functional relationship between the image coordinate system and the object coordinate system can be found. The optical sections are projected in Y-axis direction and the images of the profiles in which the optical sections locate can be obtained. According to the principle of the profile method, the MPD can be measured and the MTD can be estimated.

In conclusion, the measuring system of multi-line laser and binocular vision includes the following key points:

(1) Establishment of the mathematical model.
(2) Digital image processing.
(3) The algorithm of stereo matching.
(4) Estimation of MTD from MPD.

3. Mathematical model

According to the perspective principle of CCD cameras, the mathematical model of the measurement can be established, as shown in Figure 2:

The centre of the measuring platform is set as the origin O of a right-handed world coordinate system O-XYZ. The local-coordinates systems O_l-$X_lY_lZ_l$ (for the left camera) and O_r-$X_rY_rZ_r$ (for the right camera) are established with the optical axis of the camera lens setting as the Z axis. C_l and C_r represent the image planes of the cameras. $P_l(x_l, y_l)$ and $P_r(x_r, y_r)$ are assumed to be the image points that are corresponding to a random object point $P(X, Y, Z)$ on the contour of the optical section.

In the imaging system of the two cameras, the object points are transformed into the camera coordinate system via the world coordinate system and then converted into the image coordinate system through the Equations (1) and (2):

$$Z_{cl}\begin{bmatrix} x_l \\ y_l \\ 1 \end{bmatrix} = M_1^l M_2^l \begin{bmatrix} X \\ Y \\ Z \\ 1 \end{bmatrix} = M^l \begin{bmatrix} X \\ Y \\ Z \\ 1 \end{bmatrix} = \begin{bmatrix} m_{11}^l & m_{12}^l & m_{13}^l & m_{14}^l \\ m_{21}^l & m_{22}^l & m_{23}^l & m_{24}^l \\ m_{31}^l & m_{32}^l & m_{33}^l & m_{34}^l \end{bmatrix} \begin{bmatrix} X \\ Y \\ Z \\ 1 \end{bmatrix} \quad (1)$$

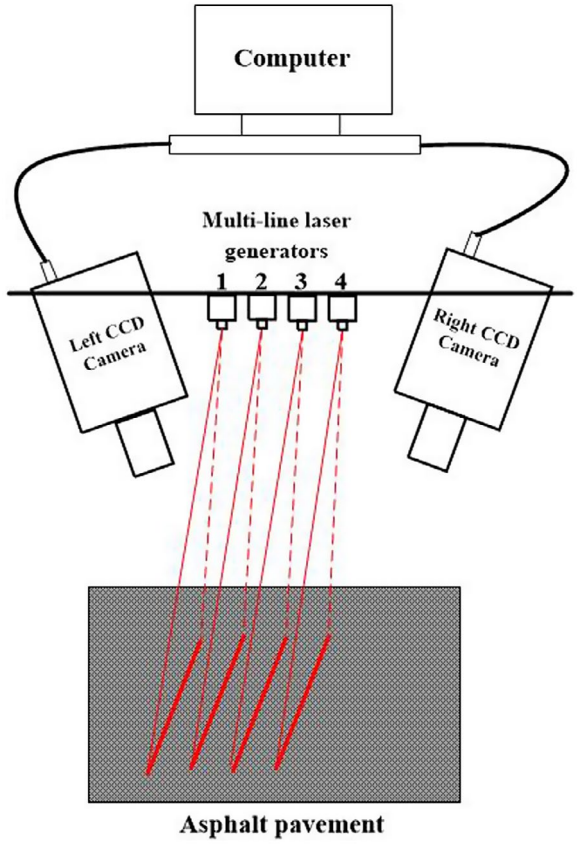

Figure 1. Measuring system of multi-line laser and binocular vision.

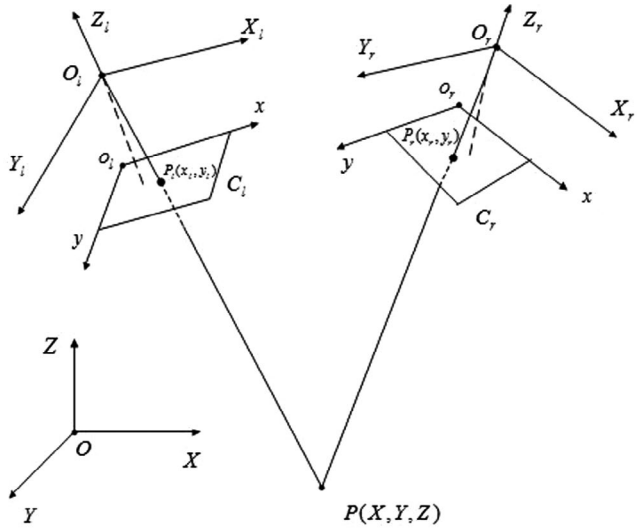

Figure 2. Mathematical model of the measurement based on multi-line laser and binocular vision.

$$Z_{cr}\begin{bmatrix} x_r \\ y_r \\ 1 \end{bmatrix} = M_1^r M_2^r \begin{bmatrix} X \\ Y \\ Z \\ 1 \end{bmatrix} = M^r \begin{bmatrix} X \\ Y \\ Z \\ 1 \end{bmatrix} = \begin{bmatrix} m_{11}^r & m_{12}^r & m_{13}^r & m_{14}^r \\ m_{21}^r & m_{22}^r & m_{23}^r & m_{24}^r \\ m_{31}^r & m_{32}^r & m_{33}^r & m_{34}^r \end{bmatrix} \begin{bmatrix} X \\ Y \\ Z \\ 1 \end{bmatrix} \quad (2)$$

$M_1^1$and M_2^1in the Equation (1) are the internal and external parameter matrices of the left camera, respectively. M^l is the projection matrix of the left camera. Similarly, M_1^r and M_2^r in the Equation (2) are the internal and external parameter matrices of the right camera. M^r is the projection matrix of the right camera. $M^1$and M^r can be calibrated directly according to the direct linear transformation method (Abdel-Aziz and Karara 1971, Tsai 1986, Qu *et al*. 2012).

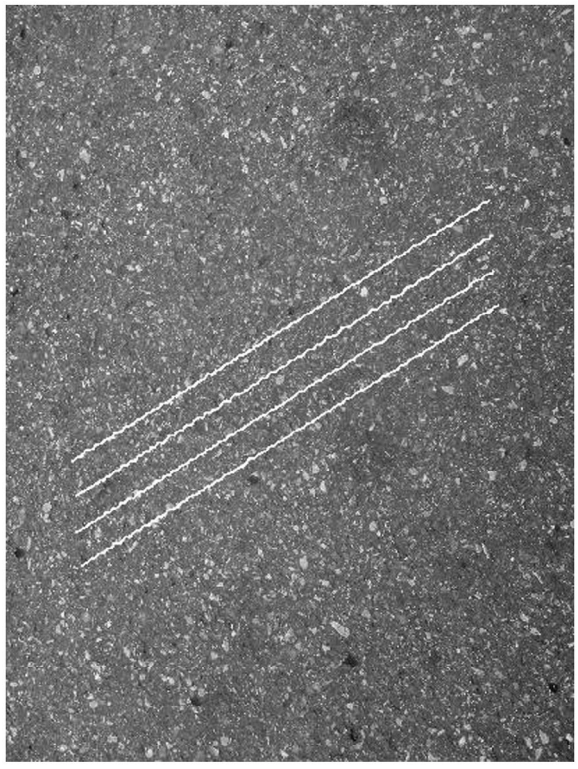

Figure 3. Original two-dimensional multi-line striation distorted image.

Further deducing the Equation (1) and the Equation (2), the image coordinate $P(X, Y, Z)$ can be obtained, as shown in Equation (3).

$$\begin{bmatrix} x_l m_{31}^l - m_{11}^l & x_l m_{32}^l - m_{12}^l & x_l m_{33}^l - m_{13}^l \\ y_l m_{31}^l - m_{21}^l & y_l m_{32}^l - m_{22}^l & v_1 m_{33}^l - m_{23}^l \\ x_r m_{31}^r - m_{11}^r & x_r m_{32}^r - m_{12}^r & x_r m_{33}^r - m_{13}^r \\ y_r m_{31}^r - m_{21}^r & y_r m_{32}^r - m_{22}^r & y_r m_{33}^r - m_{23}^r \end{bmatrix} \begin{bmatrix} X \\ Y \\ Z \end{bmatrix} = \begin{bmatrix} m_{14}^l - x_l m_{34}^l \\ m_{24}^l - y_l m_{34}^l \\ m_{14}^r - x_r m_{34}^r \\ m_{24}^r - y_r m_{34}^r \end{bmatrix} \quad (3)$$

The least square method is used to solve the Equation (3), by which the three-dimensional coordinates of the object point $P(X, Y, Z)$ on the contour of the optical section can be obtained. The profile of the optical section can be three-dimensionally reconstructed through interpolation and fitting of all the object points on it.

4. Image processing technology

Image processing is the core technology of MTD measurement based on the multi-line laser and binocular vision. The pairs of two-dimensional distorted images not only contain the striation signals modulated by the section contour, but also carry interference signals caused by ambient factors. To ensure the measuring accuracy, it is necessary to reduce noise signals and precisely extract the optical striation. Procedures of image preprocessing, threshold segmentation and extraction of striation centrelines and image coordinates are involved in this technology.

4.1. Preprocessing

The two-dimensional distorted image of the multi-line striation (as shown in Figure 3) captured by the CCD cameras can be abstracted into a two-dimensional function $f(x, y)$, which can be represented by a matrix, as shown in the Equation (4). In the Equation (4), x and y are the image coordinates; the amplitude of f of any point (x, y) is the brightness of the corresponding position on the image (Ruan *et al.* 2005).

$$f(x,y) = \begin{pmatrix} f(0,0) & f(0,1) & \cdots & f(0,N-1) \\ f(1,0) & f(1,1) & \cdots & f(1,N-1) \\ \vdots & \vdots & & \vdots \\ f(M-1,0) & f(M-1,1) & \cdots & f(M-1,N-1) \end{pmatrix} \quad (4)$$

Preprocessing is mainly to enhance resolution of the original image and remove the noise signals so as to highlight the multi-line striation signals, making the image clearer for the sake of subsequent processing. It involves the procedures of brightness transformation and spatial filtering of any point (x, y).

Brightness transformation mainly depends on the brightness value (f) of the point (x, y). The transformation function is shown as below.

$$g(x,y) = T[f(x,y)] \quad (5)$$

The function *IMADJUST* in the tool *IPT* of *MATLAB* software can be directly used to implement brightness transformation. Figure 4 shows the result of brightness transformation when $\gamma =$ 1, in which the optical striation is more obvious and conducive

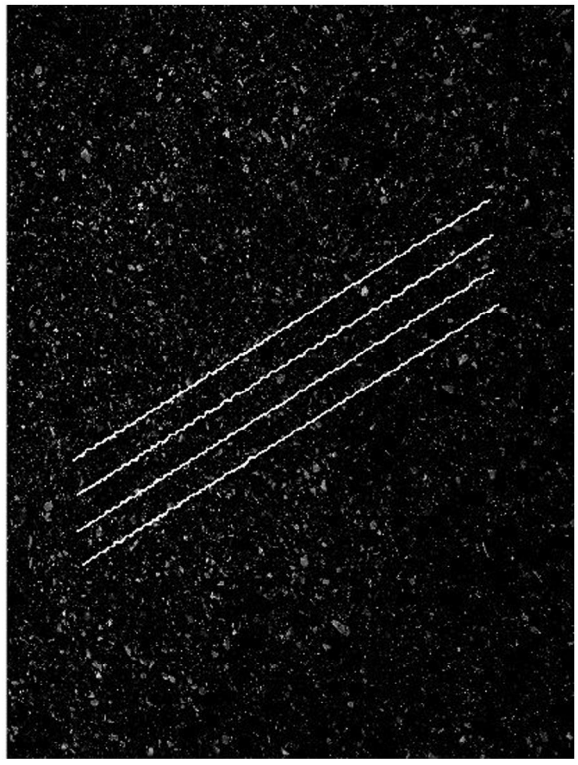

Figure 4. Brightness transformation.

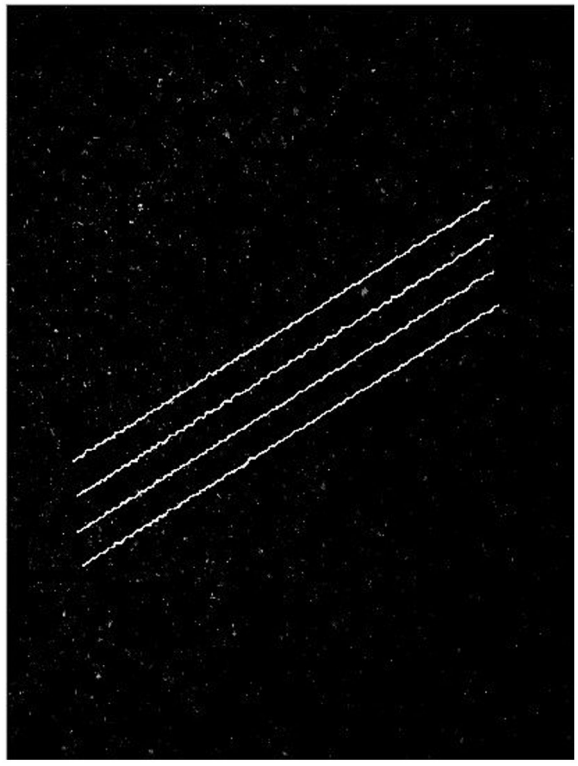

Figure 5. Median filtering.

to subsequent procedures of recognition and extraction of the target signals.

In addition, the interference of ambient light, instability of the system and vibration of devices introduce a variety of noise signals. In order to get a high precision, noise signals must be suppressed. Generally, the median filtering is a good choice for smoothing with good robustness and resolution. In the test, the median filtering image exhibited a group of smooth lines, as shown in Figure 5.

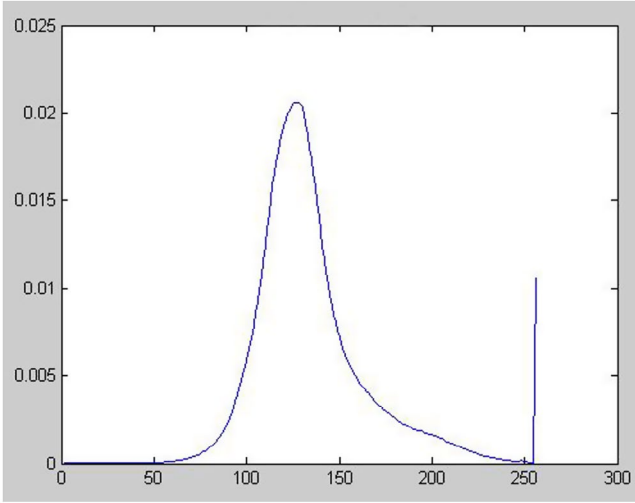

Figure 6. Grey histogram.

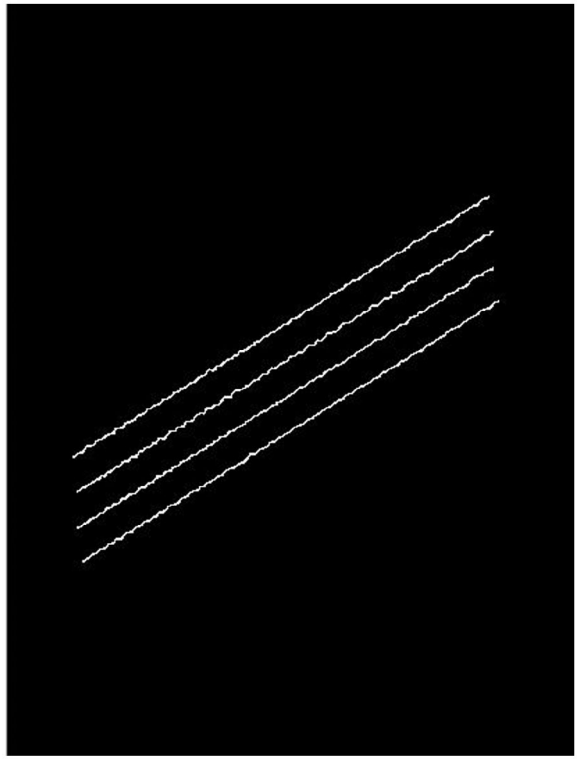

Figure 7. Threshold segmentation result.

4.2. Threshold segmentation

In the two-dimensional multi-line striation distorted image, multi-line striation is the only signal belongs to the region of interest (ROI). Therefore, it is needed to transform the greyscale image to binary image by a proper process of threshold segmentation. As the laser is the infrared light which exhibits strong contrast to asphalt pavement and the target signals just account for a small proportion, the ROI can be found out on the grey histogram and the light signal can be segmented. The grey histogram and threshold segmentation result of the distorted image are shown in Figures 6 and 7, respectively.

4.3. Extraction of the striation centreline and image coordinates

Although the striation signals are extracted after the preprocessing and threshold segmentation, the stripes on the image are too thick and uneven to be accurately positioned on the coordinate system. A further process of extraction for the striation centreline is supposed to be carried out. Refinement method, gravity method and horizontal median method are three common approaches of centreline extraction. Among them, the gravity method is selected for this procedure for its capability of accurate positioning for the Gaussian distribution centre. This method is

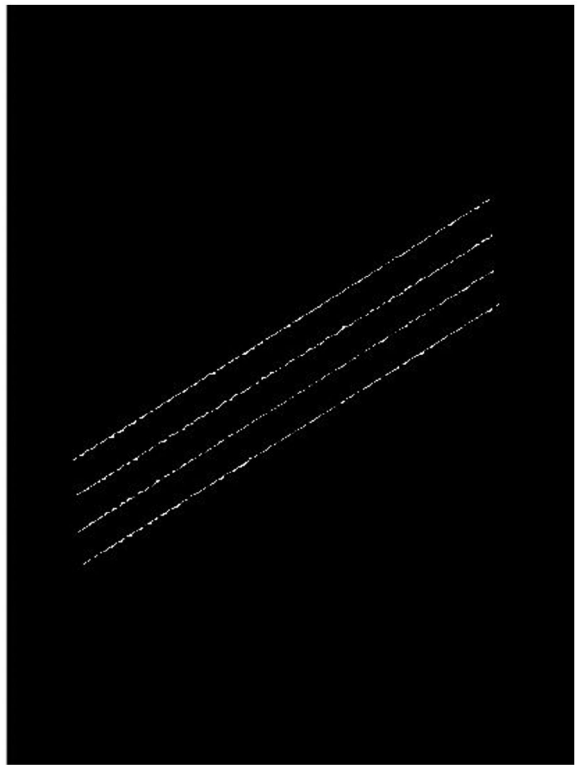

Figure 8. Centerline extraction by the gravity method.

based on the permutation of the grey level of the striations in a certain interval. The grey centroids on the abscissa represent the position of the striation centres.

Specifically, the extraction can be divided into two steps:

(1) Through binarisation, binary image matrix *BW* is obtained from the image $f(i, j)$ after threshold segmentation. The eight-neighbourhood-labelled algorithm is used to mark out k ($k = 1, 2, 3, 4, \ldots$) connected regions of the striations and define the labelling matrix L, whose dimensionality is the same as the matrix *BW*. The function *bwlabel* in the tool box *IPT* of *MATLAB* software can be used for this procedure.

(2) The sub-pixel coordinates of the centre of each row in the striation connected regions can be figured out by the gravity method. Given the ith line of non-zero interval in the kth connected region of the image matrix $f(i, j)$ is (m_k, n_k), the corresponding centre coordinate (x_k, y_k) is shown in the Equation (6):

$$\begin{cases} x_k = i \\ y_k = \dfrac{\sum_{j=m_k}^{n_k} jf(i,j)}{\sum_{j=m_k}^{n_k} f(i,j)} \end{cases} \tag{6}$$

The set of the centre coordinates (x_k, y_k) of each line in the kth connected region makes up the centreline of the kth optical striation. (x_k, y_k) is the image coordinates of the points on the striation. The image linear equation L_k^1 (or L_k^r) of the striation can be obtained by linear fitting to the image coordinates of the points on the centrelines of the kth optical striation. Figure 8 shows the effect of the centreline extraction.

5. Stereo matching algorithm

Stereo matching algorithm of the MTD measurement method based on multi-line laser and binocular vision takes the pixels on the striation centreline as the matching primitives. The matching process includes the pairing of the same striations in physical sense and the homonymous point pairs on the same striation on the image planes on both sides.

The pairing of the same striations in physical sense is implemented through the eight-neighbourhood-labelled algorithm by which the connected regions of the striations are marked out. The same marked region indicates the same striation.

The pairing of the homonymous point just needs to search for the matching point on the linear equations L_k^1 and L_k^r. According to the epipolar restriction criterion, the matching points must be located in the corresponding epipolars, which simplifies the procedure from two-dimension to one-dimension and further reduces the target range of the candidate matching points. As a result, the homonymous points locate exactly in the intersection point of the corresponding striation and epipolar.

The epipolar restriction principle is shown in Figure 9. The homonymous point $P_r(x_r, y_r)$ of the projection point $P_l(x_l, y_l)$ on the left image of a random point $P(X, Y, Z)$ on the kth striation definitely locates in the epipolar on the right image that is corresponding to P_l and cross through the right epipole e_r.

The matching principle of the homonymous point $P_r(x_r, y_r)$ of the point $P_l(x_l, y_l)$ on the kth striation of the left image is shown in Figure 10. It satisfies the Equation (7).

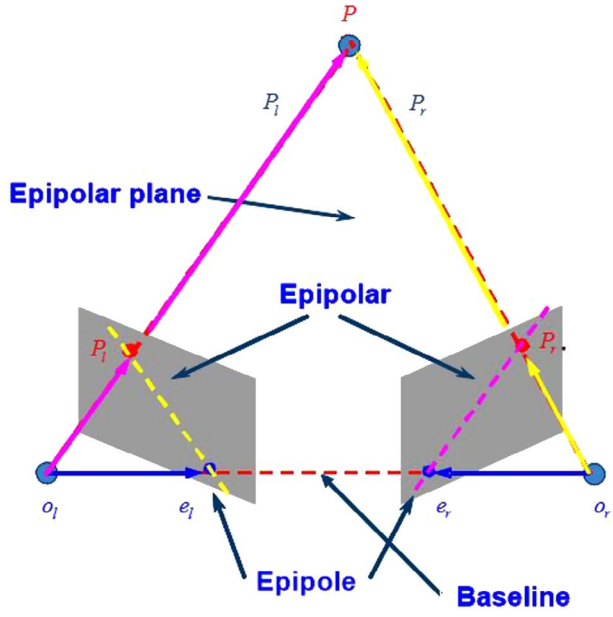

Figure 9. Centreline extraction by the gravity method.

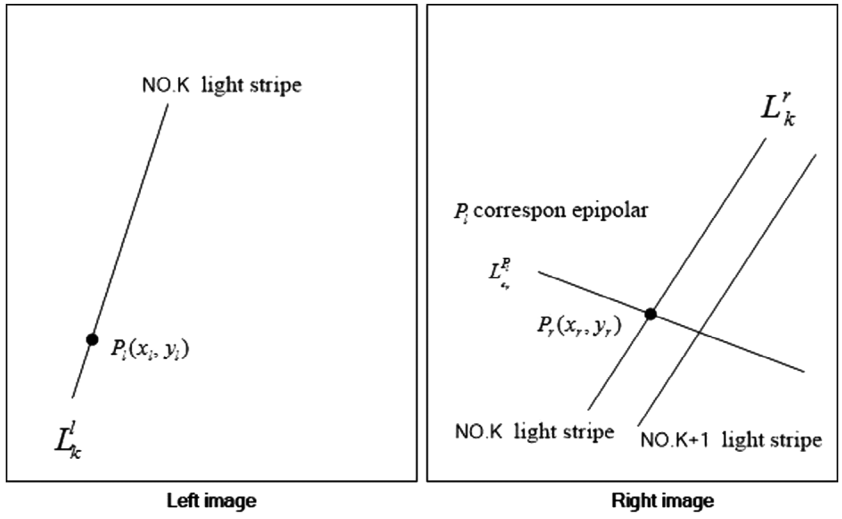

Figure 10. Principle of the homonymous points matching.

$$P_l(x_l, y_l) \in L_k^l \Rightarrow P_r(x_r, y_r) \in \begin{cases} L_k^r \\ L_{e_r}^{P_l} \end{cases} \tag{7}$$

In the Equation (7), the linear equations L_k^1 and L_k^r are obtained via the extraction of the striation centreline. The corresponding epipolar equation $L_{e_r}^{P_l}$ can be figured out as the Equation (8).

$$L_{e_r}^{P_l} = F \times \begin{bmatrix} x_l \\ y_l \\ 1 \end{bmatrix} = 0 \rightarrow L_{e_r}^{P_l}: a \times x_l + b \times y_l + c = 0 \tag{8}$$

In the Equation (8), F is a 3 × 3 fundamental matrix of the binocular vision model which is only relevant to the internal parameters and the relative position of the two CCD cameras in the model. It can be derived from the calibration matrices M^l and M^r.

6. Calculation of the MTD

Through the image processing, the three-dimensional mathematical model established and the stereo matching algorithm, the profile of the section in which the kth (k = 1, 2, 3, … m) optical striation lies can be reconstructed rapidly and accurately. Further, the MPD of the kth (k = 1, 2, 3, … m) asphalt pavement profile can be confirmed. According to the profile method, specific steps of MTD calculation are as follow:

(1) Select a 100-mm baseline from the kth optical section contour and calculate the average value of Z-coordinates of all the point on the baseline.

$$\text{avg}_k = \frac{1}{n} \sum_{i=1}^{n} Z_i \tag{9}$$

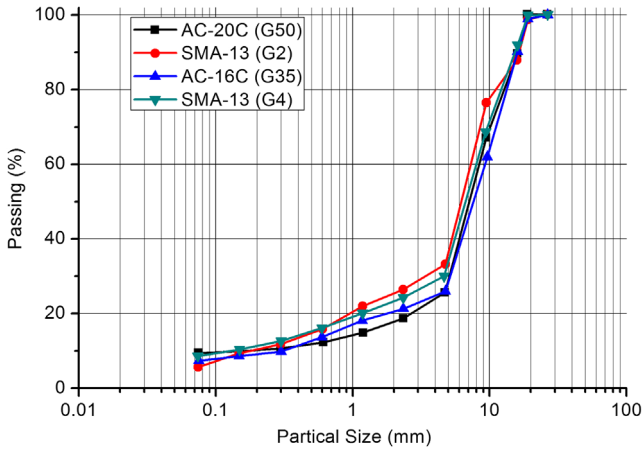

Figure 11. Aggregate grading curves of the pavement surface of the test sections.

(2) Symmetrically divide the baseline into 2 sections and, respectively, get the max Z-coordinate value Max1 and Max2 of the points in each section, then the MPD_k of this asphalt pavement profile can be figured out through the Equation (10).

$$\mathrm{MPD}_k = (\mathrm{Max1} + \mathrm{Max2})/2 - \mathrm{avg}_k \tag{10}$$

(3) Calculate the average value of all the MPD_k above to obtain the MPD of the whole pavement:

$$\mathrm{MPD} = \frac{1}{m}\sum_{k=1}^{m} \mathrm{MPD}_k \tag{11}$$

(4) Estimate MTD from MPD

MPD and MTD are both the evaluation indexes of pavement surface macro-texture. Previous researchers (Wambold *et al.* 1994) found that MPD has good linear relationship with MTD, which conform to that developed by ASTM E1845, as shown in Equation (12).

$$\mathrm{MPD} = f(\mathrm{MPD}) = 0.8 \times \mathrm{MPD} + 0.2 \tag{12}$$

7. Field tests

A set of field tests was implemented in order to verify reliability of the new measurement method, in which the sand patch test functions as the reference standard. A total of 4 km long test sections on 4 expressways (1 km for each) with different kinds of pavement materials were taken as the samples in this article. The expressways located in Shandong (G2, G35) and Hubei (G4, G50), respectively. The test points were laid out according to a separation of 2 m. The test section of G2 Expressway uses SMA-13 as the material of pavement surface, of which the asphalt-aggregate ratio is 6%, the mineral powder content is 8%. The test section of G35 Expressway uses AC-16C as the material of pavement surface, of which the asphalt-aggregate ratio is 4.5%, the mineral powder content is 3.5%. The test section of G4 Expressway uses SMA-13 as the material of pavement surface, of which the asphalt-aggregate ratio is 5.2%, the mineral powder content is 4%. The test section of G50 Expressway uses AC-20C as the material of pavement surface, of which the asphalt-aggregate ratio is 4.8%, the mineral powder content is 1%. The aggregate grading of the two pavement materials are shown in Figure 11, respectively. All the tests were conducted under similar weather and atmospheric conditions, which were sunny in winter with the illumination intensity of about 6000–8000 lx.

7.1. The measurement method based on multi-line laser and binocular vision

Taking one measure point on the G2 Expressway in Shandong for example, the original image pair acquired based on multi-line laser and binocular vision and the four profile images reconstructed are, respectively, shown in Figures 12 and 13. The light source was gas laser.

Table 1 exhibits the sample data and the calculation process of MTD on the selected test point.

7.2. Sand patch test

The sand patch test is to sand the road on the test points using standard sand, and measure the area of the sand round (as shown in Figure 14) formed on pavement surface. The ratio of the sand volume to the sand round area is exactly the value of MTD, as shown in the Equation (9).

$$\mathrm{MTD} = \frac{1000\,\mathrm{V}}{\pi D^2/4} \tag{13}$$

7.3. Results analyses

The values of the MTDs from two measurement methods present a perfect linear correlation, as shown in Figure 15–18. Each ordinate and abscissa of the scatter plots represents the value of MTD for the two methods at one test point, respectively. The high correlation coefficients have confirmed reliability of the laser-vision based measuring method.

8. Conclusions

The proposed measurement method meets the need to measure the MTD of asphalt pavement both in field and in laboratory according to ASTM standards. The profile method and the image

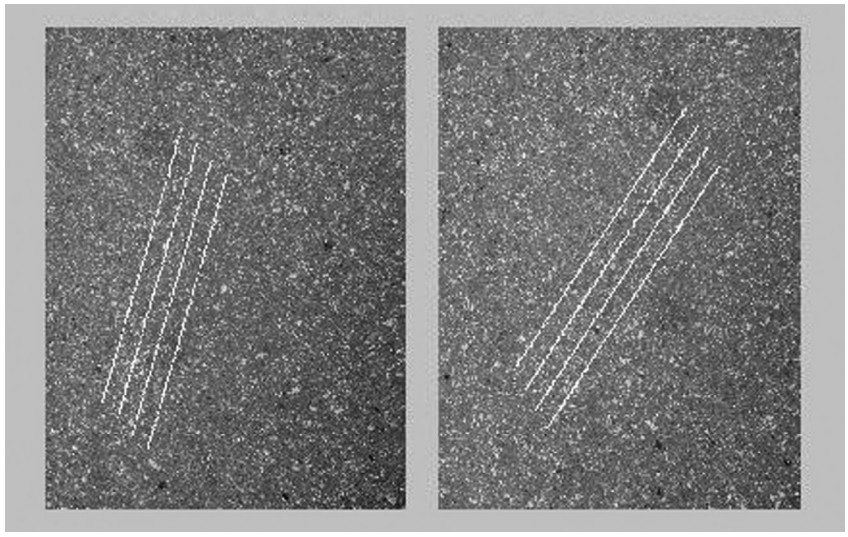

Figure 12. Original image pair.

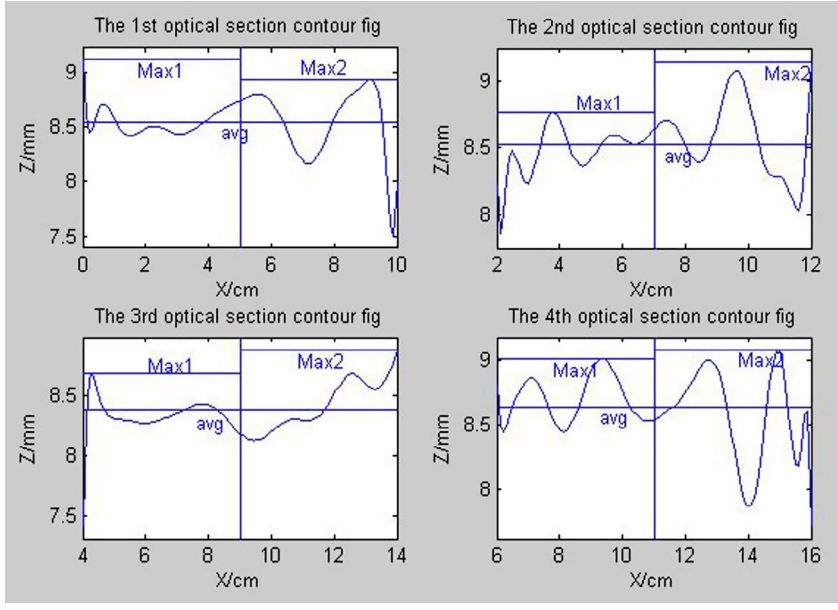

Figure 13. Profile images.

Table 1. The MTD calculation.

k parameter (mm)	No.1 profile $k = 1$	No.2 profile $k = 2$	No.3 profile $k = 3$	No.4 profile $k = 4$
avg_k	8.5396	8.5205	8.3711	8.6364
Max1	8.9351	8.7612	8.6737	9.0173
Max2	9.1175	9.1430	8.8749	9.0809
MPD_k	0.4867	0.4316	0.4031	0.4126
MPD	$\frac{1}{4}(0.4867 + 0.4316 + 0.4031 + 0.4126) = 0.4335$			
MTD	$0.8MPD + 0.2 = 0.5468$			

processing technology constitute the theoretical foundation of the proposed method. Multi-line laser and binocular vision are the core techniques that have been applied in the measurement. To be specific, the eight-neighbourhood-labelled algorithm and the gravity method are applied in this study for the extraction of multi-line laser striation centrelines. The combinative technology of multi-line laser paring and epipolar restriction was put forward in order to achieve fast matching of binocular vision. The feasibility of the method is expounded with the description of the theoretical system of this study, including the mathematical model, the image processing and the stereo matching algorithm. The three-dimensional reconstruction of the optical section profiles is implemented.

MTD was estimated through MPD according to the principle of the profile method. A set of field tests was carried out to verify

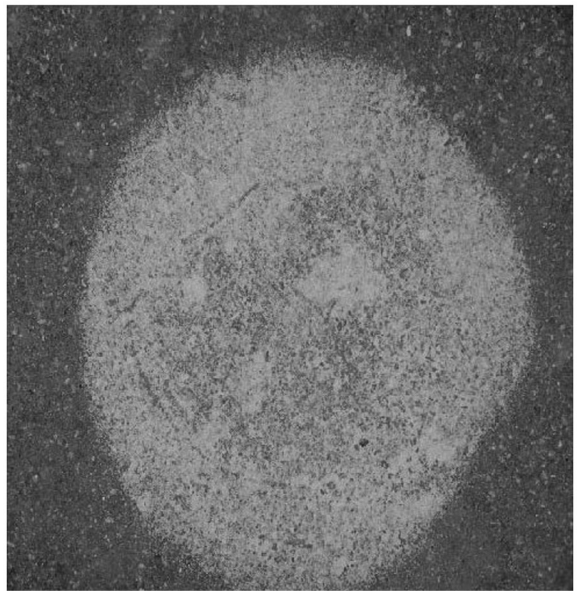

Figure 14. The sand round.

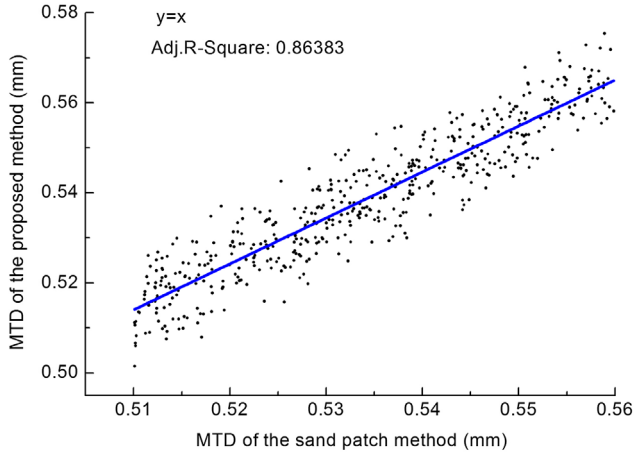

Figure 15. The MTD correlation between the two methods (G2 Expressway, Shandong).

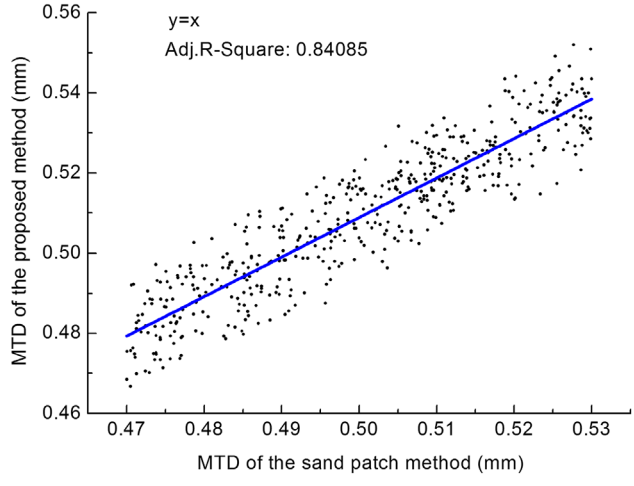

Figure 16. The MTD correlation between the two methods (G35 Expressway, Shandong).

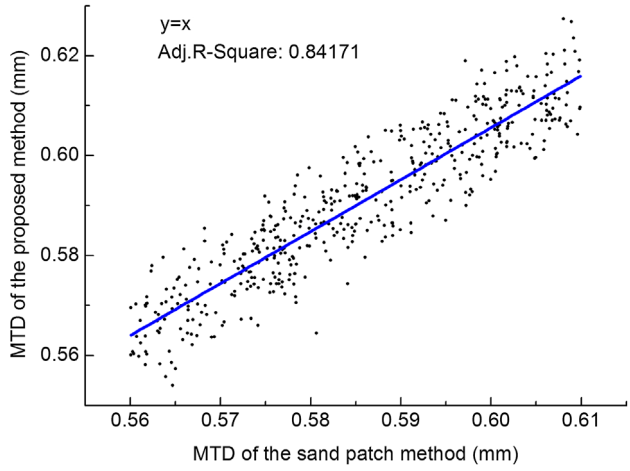

Figure 17. The MTD correlation between the two methods (G4 Expressway, Hubei).

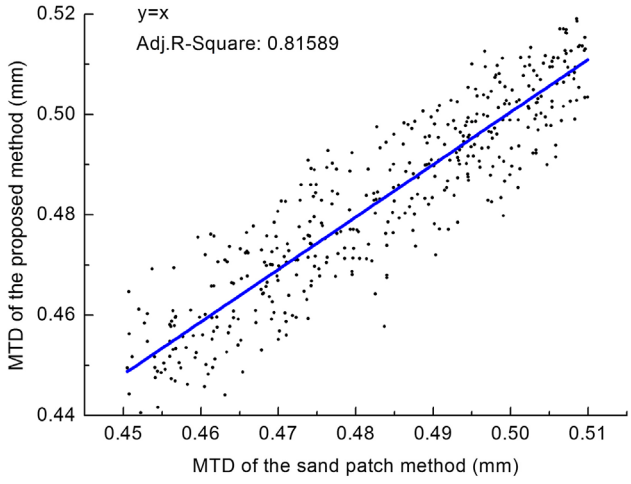

Figure 18. The MTD correlation between the two methods (G50 Expressway, Hubei).

reliability of the developed measurement method. The result of the advanced method shows good consistency with the sand patch method.

Disclosure statement

No potential conflict of interest was reported by the authors.

Funding

This work was supported by the National Natural Science Foundations of China [grant number 51479105], [grant number 51279094], [grant number 51078222], [grant number 50978207]; the Natural Science Foundations of Shandong Province of China [grant number ZR2011EEM012], [grant number ZR2013EEQ025]; the Fundamental Research Funds for the Central Universities of China [grant number 2014YQ013], the Program for New Century Excellent Talents in University of Ministry of Education of China [grant number NCET-13-0340] and the Independent Innovation Foundation of Shandong University (IIFSDU) [grant number 2012HW003].

References

Abdel-Aziz, Y.I., 1971. Direct linear transformation from comparator coordinates into object space coordinates in close-range photogrammetry. *ASP Symp. on Close-Range Photogram*, (5), 103–107.

Abe, H., Henry, J.J., Tamai, A., and Wambold, J., 2001. Measurement of pavement macrotexture with circular texture meter. *Transportation Research Record: Journal of the Transportation Research Board*, 1764, 201–209.

Adams, J.M. and Richard Kim, Y., 2014. Mean profile depth analysis of field and laboratory traffic-loaded chip seal surface treatments. *International Journal of Pavement Engineering*, 15 (7), 645–656.

ASTM E1845-09, 2009. *Standard practice of the calculating pavement macrotexture mean profile depth*. West Conshohocken, PA: American Society for Testing and Materials.

ASTM, E 2157–01, 2001. *Road and paving materials; vehicle-pavement systems*. West Conshohocken, PA: Annual Book of ASTM Standards.

Byrum, C.R., *et al.*, 2010. Experimental short-wavelength surface textures in Portland cement concrete pavements. *Transportation Research Record: Journal of the Transportation Research Board*, 2155, 170–178.

Choubane, B., McNamara, R.L., and Page, G.C., 2002. Evaluation of high-speed profilers for measurement of asphalt pavement smoothness in Florida. *Transportation Research Record: Journal of the Transportation Research Board*, 1813, 62–67.

El Gendy, A. and Shalaby, A., 2007. Mean profile depth of pavement surface macrotexture using photometric stereo techniques. *Journal of Transportation Engineering*, 133 (7), 433–440.

El Gendy, A. and Shalaby, A., 2008. Image requirements for three-dimensional measurements of pavement macrotexture. *Transportation Research Record: Journal of the Transportation Research Board*, 2068, 126–134.

El Gendy, A., *et al.*, 2011. Stereo-vision applications to reconstruct the 3D texture of pavement surface. *International Journal of Pavement Engineering*, 12 (3), 263–273.

Ergun, M., Lyinam, S., and Lyinam, A.F., 2005. Prediction of road surface friction coefficient using only macro- and microtexture measurements. *Journal of Transportation Engineering*, 131 (4), 311–319.

Flintsch, G.W., Huang, M., and McGhee, K., 2005. Harmonization of macrotexture measuring devices. *Journal of ASTM International*, 2 (9), 47–58.

Flintsch, G.W., *et al.*, 2003. Pavement surface macrotexture measurement and applications. *Transportation Research Record: Journal of the Transportation Research Board*, 1860, 168–177.

Hanson, D.I. and Prowell, B.D., 2004. *Evaluation of circular texture meter for measuring surface texture of pavements*. Auburn, AL: National Center for Asphalt Technology, NCAT Report 04-05.

Henry, J.J., 2000. Evaluation of pavement friction characteristics. NCHRP Synthesis 291. Washington, DC: Transportation Research Board, National Research Council.

McGhee, K.K. and Flintsch, G.W., 2003. High-speed texture measurement of pavements. Charlottville, VA: VAes, Virginia Transportation Research Council (VTRC) Report 03-R9, VTRC.

Meegoda, J.N., *et al.*, 2013. Pavement texture from high-speed laser for pavement management system. *International Journal of Pavement Engineering*, 14 (8), 697–705.

Noyce, D.A., *et al.*, 2007. Incorporating road safety into pavement management: maximizing asphalt pavement surface friction for road safety improvements. Wisconsin: Midwest Regional University Transportation Center, MRUTC04-04, Report No. 2007-005.

Pidwerbesky, B., *et al.*, 2006. *Road surface texture measurement using digital image processing and information theory*. Wellington: Land Transport New Zealand Research, Report: 290.

Prowell, B.D. and Hanson, D.I., 2005. Evaluation of circular texture meter for measuring surface texture of pavements. *Transportation Research Record: Journal of the Transportation Research Board*, 1929, 88–96.

Ruan, Qiu-qi, *et al.*, translation, 2005. Digital Image Processing Using MATLAB. Beijing: Beijing Electronic Industry Press, 9.

Qu, Xue-jun, Song, Yue-wen, and Wang, Yong, 2012. 3D measurement method based on binocular vision and linear structured light. *Advanced Materials Research*, 422, 17–23.

Tsai, R.Y., 1986. *An efficient and accurate camera calibration technique for 3D machine vision. In: Proceedings IEEE conference on computer vision and pattern recognition*, Seattle.

Vercoe, J., 2002. *Chip seal texture measurement by high speed laser*. Research Report. Christchurch: Fulton Hogan .

Wambold, J.C. and Henry, J.J., 1994. International PIARC experiment to compare and harmonize texture and skid resistance measurement. Stockholm: Nordic Road and Transport Research.

Zelelew, H.M., Papagiannakis, A.T., and de León Izeppi, E.D., 2013. Pavement macro-texture analysis using wavelets. *International Journal of Pavement Engineering*, 14 (8), 725–735.